Research Article | Vol. 24, No. 16 | 8 Aug 2016 | OPTICS EXPRESS 18468

Optics EXPRESS

High efficiency double-wavelength dielectric metasurface lenses with dichroic birefringent meta-atoms

EHSAN ARBABI, AMIR ARBABI, SEYEDEH MAHSA KAMALI, YU HORIE, AND ANDREI FARAON*

T. J. Watson Laboratory of Applied Physics, California Institute of Technology, 1200 E. California Blvd., Pasadena, California 91125, USA

*faraon@caltech.edu

Abstract: Metasurfaces are ultrathin optical structures that manipulate optical wavefronts. Most metasurface devices which deflect light are designed for operation at a single wavelength, and their function changes as the wavelength is varied. Here we propose and demonstrate a double-wavelength metasurface based on polarization dependent dielectric meta-atoms that control the phases of two orthogonal polarizations independently. Using this platform, we design lenses that focus light at 915 and 780 nm with perpendicular linear polarizations to the same focal distance. Lenses with numerical apertures up to 0.7 and efficiencies from 65% to above 90% are demonstrated. In addition to the high efficiency and numerical aperture, an important feature of this technique is that the two operation wavelengths can be chosen to be arbitrarily close. These characteristics make these lenses especially attractive for fluorescence microscopy applications.

OCIS codes: (050.6624) Subwavelength structures; (050.1965) Diffractive lenses; (220.1000) Aberration compensation; (050.2555) Form birefringence.

References and links

1. A. V. Kildishev, A. Boltasseva, and V. M. Shalaev, "Planar photonics with metasurfaces," Science **339**, 1232009 (2013).
2. N. Yu and F. Capasso, "Flat optics with designer metasurfaces," Nature Mater. **13**, 139–150 (2014).
3. S. Jahani and Z. Jacob, "All-dielectric metamaterials," Nature Nanotech. **11**, 23–36 (2016).
4. P. Lalanne, S. Astilean, P. Chavel, E. Cambril, and H. Launois, "Blazed binary subwavelength gratings with efficiencies larger than those of conventional echelette gratings," Opt. Lett. **23**, 1081–1083 (1998).
5. S. Astilean, P. Lalanne, P. Chavel, E. Cambril, and H. Launois, "High-efficiency subwavelength diffractive element patterned in a high-refractive-index material for 633 nm," Opt. Lett. **23**, 552–554 (1998).
6. P. Lalanne, S. Astilean, P. Chavel, E. Cambril, and H. Launois, "Design and fabrication of blazed binary diffractive elements with sampling periods smaller than the structural cutoff," J. Opt. Soc. Am. A **16**, 1143–1156 (1999).
7. D. Fattal, J. Li, Z. Peng, M. Fiorentino, and R. G. Beausoleil, "Flat dielectric grating reflectors with focusing abilities," Nature Photon. **4**, 466–470 (2010).
8. D. Lin, P. Fan, E. Hasman, and M. L. Brongersma, "Dielectric gradient metasurface optical elements," Science **345**, 298–302 (2014).
9. A. Arbabi, M. Bagheri, A. J. Ball, Y. Horie, D. Fattal, and A. Faraon, "Controlling the phase front of optical fiber beams using high contrast metastructures" in *CLEO: Science and Innovations*, OSA Technical Digest (online) (Optical Society of America, 2014), paper STu3M.4.
10. S. Vo, D. Fattal, W. V. Sorin, P. Zhen, T. Tho, M. Fiorentino, and R. G. Beausoleil, "Sub-wavelength grating lenses with a twist," IEEE Photonics Technol. Lett. **26**, 1375–1378 (2014).
11. A. Arbabi, Y. Horie, A. J. Ball, M. Bagheri, and A. Faraon, "Subwavelength-thick lenses with high numerical apertures and large efficiency based on high-contrast transmitarrays," Nat. Commun. **6**, 7069 (2015).
12. A. Arbabi, Y. Horie, M. Bagheri, and A. Faraon, "Dielectric metasurfaces for complete control of phase and polarization with subwavelength spatial resolution and high transmission," Nature Nanotech. **10**, 937–943 (2015).
13. P. R. West, J. L. Stewart, A. V. Kildishev, V. M. Shalaev, V. V. Shkunov, F. Strohkendl, Y. A. Zakharenkov, R. K. Dodds, and R. Byren, "All-dielectric subwavelength metasurface focusing lens," Opt. Express **22**, 26212–26221 (2014).
14. M. Decker, I. Staude, M. Falkner, J. Dominguez, D. N. Neshev, I. Brener, T. Pertsch, and Y. S. Kivshar, "High-efficiency dielectric huygens' surfaces," Adv. Opt. Mater. **3**, 813–820 (2015).

#267421 http://dx.doi.org/10.1364/OE.24.018468
Journal © 2016 Received 2 Jun 2016; revised 23 Jul 2016; accepted 25 Jul 2016; published 3 Aug 2016

Optics EXPRESS

15. Y. F. Yu, A. Y. Zhu, R. Paniagua-Dominguez, Y. H. Fu, B. Luk'yanchuk, and A. I. Kuznetsov, "High-transmission dielectric metasurface with 2π phase control at visible wavelengths," Laser Photon. Rev. **9**, 412–418 (2015).
16. A. Arbabi, R. M. Briggs, Y. Horie, M. Bagheri, and A. Faraon, "Efficient dielectric metasurface collimating lenses for mid-infrared quantum cascade lasers," Opt. Express **23**, 33310–33317 (2015).
17. S. Campione, L. I. Basilio, L. K. Warne, and M. B. Sinclair, "Tailoring dielectric resonator geometries for directional scattering and huygens' metasurfaces," Opt. Express **23**, 2293–2307 (2015).
18. M. I. Shalaev, J. Sun, A. Tsukernik, A. Pandey, K. Nikolskiy, and N. M. Litchinitser, "High-efficiency all-dielectric metasurfaces for ultracompact beam manipulation in transmission mode," Nano Lett. **15**, 6261–6266 (2015).
19. S. M. Kamali, A. Arbabi, E. Arbabi, Y. Horie, and A. Faraon, "Decoupling optical function and geometrical form using conformal flexible dielectric metasurfaces," Nat. Commun. **7**, 11618 (2016).
20. S. M. Kamali, E. Arbabi, A. Arbabi, Y. Horie, and A. Faraon, "Highly tunable elastic dielectric metasurface lenses," arXiv:1604.03597 (2016).
21. A. Faraon, A. Arbabi, Y. Horie, E. Arbabi, and S. M. Kamali, "Flat free-space optical elements based on dielectric metasurfaces," SPIE Newsroom, http://spie.org/newsroom/6375-flat-free-space-optical-elements-based-on-dielectric-metasurfaces?ArticleID=x117825.
22. Y. Ren, L. Li, Z. Wang, S. M. Kamali, E. Arbabi, A. Arbabi, Z. Zhao, G. Xie, Y. Cao, N. Ahmed, Y. Yan, C. Liu, A. J. Willner, S. Ashrafi, M. Tur, A. Faraon, and A. E. Willner, "Orbital angular momentum-based space division multiplexing for high-capacity underwater optical communications," arXiv:1604.06865 (2016).
23. M. Born and E. Wolf, *Principles of Optics: Electromagnetic Theory of Propagation, Interference and Diffraction of Light* (Cambridge University ,1999).
24. D. C. O'Shea, T. J. Suleski, A. D. Kathman, and D. W. Prather, *Diffractive Optics: Design, Fabrication, and Test* (SPIE, 2004).
25. F. Aieta, M. A. Kats, P. Genevet, and F. Capasso, "Multiwavelength achromatic metasurfaces by dispersive phase compensation," Science **347**, 1342–1345 (2015).
26. E. Arbabi, A. Arbabi, S. M. Kamali, Y. Horie, and A. Faraon, "Multiwavelength polarization-insensitive lenses based on dielectric metasurfaces with meta-molecules," Optica **3**, 628–633 (2016).
27. O. Eisenbach, O. Avayu, R. Ditcovski, and T. Ellenbogen, "Metasurfaces based dual wavelength diffractive lenses," Opt. Express **23**, 3928–3936 (2015).
28. M. Khorasaninejad, F. Aieta, P. Kanhaiya, M. A. Kats, P. Genevet, D. Rousso, and F. Capasso, "Achromatic metasurface lens at telecommunication wavelengths," Nano Lett. **15**, 5358–5362 (2015).
29. Z. Zhao, M. Pu, H. Gao, J. Jin, X. Li, X. Ma, Y. Wang, P. Gao, and X. Luo, "Multispectral optical metasurfaces enabled by achromatic phase transition," Sci. Rep. **5**, 15781 (2015).
30. M. P. Backlund, A. Arbabi, P. N. Petrov, E. Arbabi, S. Saurabh, A. Faraon, and W. E. Moerner, "Removing orientation-induced localization biases in single-molecule microscopy using a broadband metasurface mask," Nature Photon. **10**, 459–462 (2016).
31. V. Liu and S. Fan, "S4 : A free electromagnetic solver for layered periodic structures," Comput. Phys. Commun. **183**, 2233–2244 (2012).
32. P. Lalanne, "Waveguiding in blazed-binary diffractive elements," J. Opt. Soc. Am. A **16**, 2517–2520 (1999).
33. D. B. Murphy and M. W. Davidson, *Fundamentals of Light Microscopy and Electronic Imaging, 2nd ed.* (Wiley-Blackwell, 2012).
34. A. Arbabi, E. Arbabi, S. M. Kamali, Y. Horie, S. Han, and A. Faraon, "An optical metasurface planar camera," arXiv:1604.06160 (2016).

Metasurfaces are two-dimensional arrangements of sub-wavelength optical scatterers designed to control the amplitude, phase, and polarization of light [1–8]. Among these, high contrast dielectric metasurfaces have proven to be very versatile due to their high efficiency and ability to control phase and polarization of light with subwavelength resolution on both planar and non-planar surfaces in different parts of the optical spectrum [9–22]. Similar to other diffractive optical elements, metasurfaces with deflection capabilities such as lenses and beam deflectors suffer from chromatic aberrations [23–26], as schematically shown in Fig. 1(a). Multi-wavelength metasurface lenses have been demonstrated using several techniques including polarization and wavelength selectivity of plasmonic nano-scatterers [27], aperiodic arrays of coupled dielectric resonators [25, 28], generating a hologram with the combined phase profiles for multiple wavelengths [29], and using metamolecules formed from combining multiple meta-atoms [26]. However, lenses demonstrated by these methods have multiple focuses at each wavelength [25, 27–29] or have low efficiency at least at some of the wavelengths [25–29]. In addition, although the metamolecule technique used in [26] results in a single focus at each wavelength, the corrected wavelengths cannot be very close. Here we demonstrate double-wavelength

Optics EXPRESS

dielectric metasurface lenses that focus two wavelengths of light with perpendicular linear polarizations to the same focal distance, as schematically shown in Fig. 1(b) (e.g. the x-polarized light at a wavelength λ_1 and y-polarized light at a different wavelength λ_2 are focused to the same distance). We experimentally demonstrate lenses with large numerical apertures (NA values up to 0.7) and high efficiencies at both wavelengths ($\eta \sim 65\% - 92\%$) with nearly diffraction-limited operation. In addition to lenses, this concept can be applied to other metasurfaces to independently control the wavefronts at two different wavelengths for orthogonal polarizations, and provide different functionalities at those wavelengths.

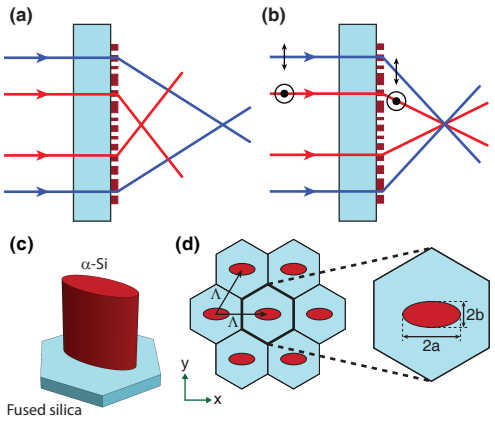

Fig. 1. (a) Normal chromatic dispersion of a metasurface lens, resulting in different focal distances for different wavelengths (schematically shown by red and blue rays), and (b) schematics of a metasurface corrected to focus light with two different wavelengths and orthogonal linear polarizations to the same focal distance. (c) An α-Si nano-post with elliptical cross-section exhibiting birefringence. (d) A metasurface formed by arraying elliptical nano-posts in a periodic lattice.

We have previously shown that metasurfaces based on amorphous silicon (α-Si) nano-posts with elliptical cross sections [Fig. 1(c)] can independently control the phases of two orthogonal polarizations at a single wavelength [12]. These metasurfaces are composed of nano-posts placed at the vertices of a hexagonal lattice shown in Fig. 1(d). For proper choices of the lattice constant ($\sim 0.5\lambda$) and the height of the nano-posts ($\sim 0.6\lambda$), the phase of light for two linear polarizations oriented along the nano-post axes can be controlled independently by changing the ellipse diameters [12]. We have also demonstrated broadband operation of non-deflecting metasurfaces (e.g. spatially varying wave plates) composed of elliptical nano-posts [30], but the approach is not applicable to the metasurfaces operating based on light deflection (e.g. lenses). Here we show that the two control parameters (i.e. the axis lengths) of nano-posts with elliptical cross-sections can be utilized to independently control the wavefronts of optical waves with two different wavelengths and orthogonal polarizations. For instance, the phase profile of the device can be independently controlled for x-polarized light at a wavelength λ_1, and for y-polarized light at a different wavelength λ_2. The behavior of the device for cross polarized light (e.g. y-polarized light at λ_1) will be governed through the regular chromatic dispersion of diffractive devices (see for instance [23, 26]).

Figures 2(a) and 2(b) show simulated transmission amplitude (top) and phase (bottom) at 915 and 780 nm for x and y-polarized light, respectively (ellipse diameters $2a$ and $2b$ and the axis directions are shown in Fig. 1(d)). Here, the meta-atoms are assumed to be 553 nm tall, the lattice constant is 500 nm, and the wavelengths are chosen to match available laser sources in our lab. Rigorous coupled wave analysis (RCWA) was used for the simulations [31]. The

Optics EXPRESS

nano-posts operate as truncated multimode optical waveguides with multiple resonances around the operation wavelengths [11, 19, 32]. The ellipticity, results in an effective birefringence and a phase difference for light polarized along the two axes of the ellipse [12]. Therefore, the two ellipse diameters provide two phase control parameters that enable independent control of phase for light polarized along the two axes [12]. Figure 2 shows that the independent phase control is possible even if the two orthogonal polarizations of light have different wavelengths. Using the simulated transmission amplitude and phase data, we find the corresponding ellipse diameters that provide any desired phase pairs at both wavelengths, ϕ_1 and ϕ_2, while keeping both transmission amplitudes high. To simultaneously achieve the desired phases and high transmission amplitudes at both wavelengths, we minimize the total complex amplitude error defined as $\varepsilon = |\exp(i\phi_1) - t_1|^2 + |\exp(i\phi_2) - t_2|^2$. Here ϕ_1 and ϕ_2 are the desired phases at the two wavelengths, and t_1 and t_2 are complex transmissions of nano-posts at the two wavelengths for the corresponding orthogonal linear polarizations. The corresponding values of the chosen diameters are plotted in Fig. 2(c) as functions of the phases at the two wavelengths. As Fig. 2(c) shows, the axis length $2a$ dominantly controls the phase of x-polarized light, and the phase of y-polarized light is mostly controlled by the axis length $2b$. Amplitudes and phases of these chosen nano-posts are plotted in Figs. 2(d) and 2(e), showing that this independent phase control is achieved with very high accuracy and high transmission. Using this independent control, any two arbitrary phase profiles for orthogonal linearly polarized light at the two wavelengths can be realized.

We designed, fabricated, and characterized five lenses with the same diameter of 200 μm and numerical apertures ranging from 0.12 to 0.7 that simultaneously work at 915 and 780 nm, for x and y-polarized light, respectively. The fabrication process was similar to [12]: a 553 nm α-Si layer was deposited on a fused silica substrate using plasma enhanced vapor deposition. The metasurface pattern was generated with an electron beam lithography system. A $\sim$70 nm aluminum oxide layer was deposited using electron beam evaporation, and was lifted off, leaving a hard mask defining the nano-posts. The hard mask was used to etch the α-Si layer in a dry etching step, and was then removed. Scanning electron microscope images of the fabricated devices are shown in Fig. 3.

Figure 4 shows schematics of the measurement setups used to characterize the devices. A custom built microscope with a $\sim$100$\times$ magnification, shown schematically in Fig. 4(a), was used to perform the intensity distribution measurements. Figure 5 summarizes the measurement results for the five lenses. Axial and focal plane intensities are plotted in Figs. 5(a) and 5(b) for 780 and 915 nm, respectively. At both wavelengths and for all lenses, one single focus is observed close to the designed distances of 100, 200, 400, 600, and 800 μm. As denoted by Fig. 5(c), all lenses have a nearly diffraction limited focus (measured FWHMs at both wavelengths and for all NA values are less than 7% larger than their diffraction limited values). The measured FWHMs in the axial plane are plotted in Fig. 5(d), along with the theoretical values calculated from $2\pi w^2/\lambda$, with w denoting the diffraction limited transverse FWHM. Efficiency was defined as the measured power in focus, divided by the total power incident on the lens. The setup used to measure the efficiencies is schematically shown in Fig. 4(b). Since the diameter of the collimated beam ($\sim$2.3 mm, using the $1/e^2$ intensity definition) is much larger than the size of the metasurface lenses, for efficiency measurements the beam was partially focused using a lens with a focal distance of 200 mm to have a diameter of $\sim$134 μm at the metasurface lenses (such that 99% of the beam power passes through the lens aperture). The radius of curvature of the beam at the metasurfaces is $\sim$16 mm, which is much larger than the focal distances of the metasurface lenses, making the curvature of the beam almost negligible. The measured efficiencies are plotted in Fig. 5(e) for both wavelengths, and are seen to be above 65% for all NAs at both wavelengths. Similar to our previous works [11], efficiency generally decreases with increasing NA. A set of fabricated pinholes were used to filter out-of-focus light for efficiency

Optics EXPRESS

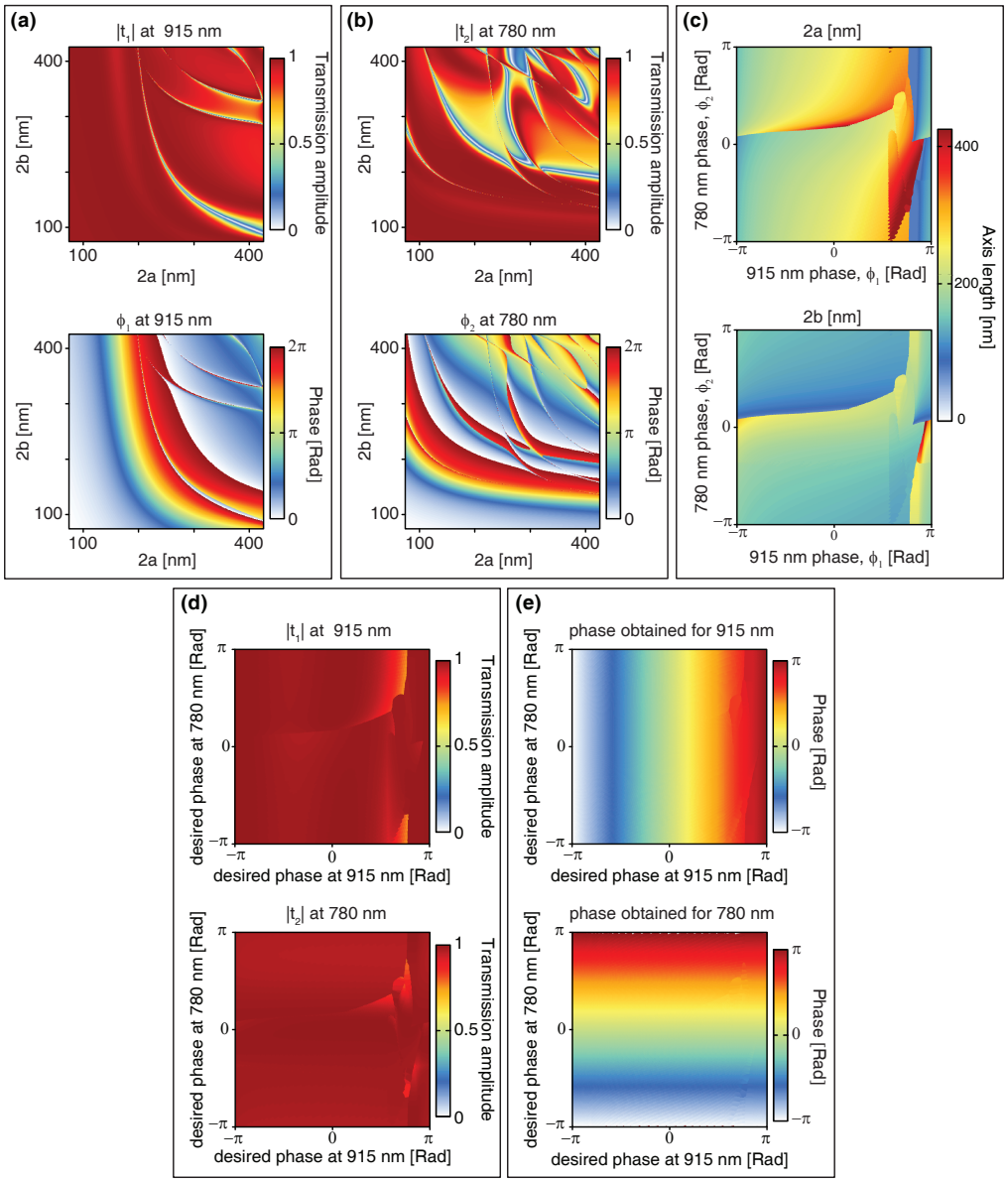

Fig. 2. (a) Transmission amplitude (top) and phase (bottom) of the meatasurface at 915 nm for *x*-polarized light versus ellipse diameters. (b) The same plots as (a), but for *y*-polarized light at 780 nm. (c) Optimal values of diameters $2a$ and $2b$ that provide phase pairs (ϕ_1, ϕ_2) for complete phase coverage at the two wavelengths. (d) Transmission amplitude, and (e) phase at both wavelengths for the corresponding optimal diameters shown in (c).

Optics EXPRESS

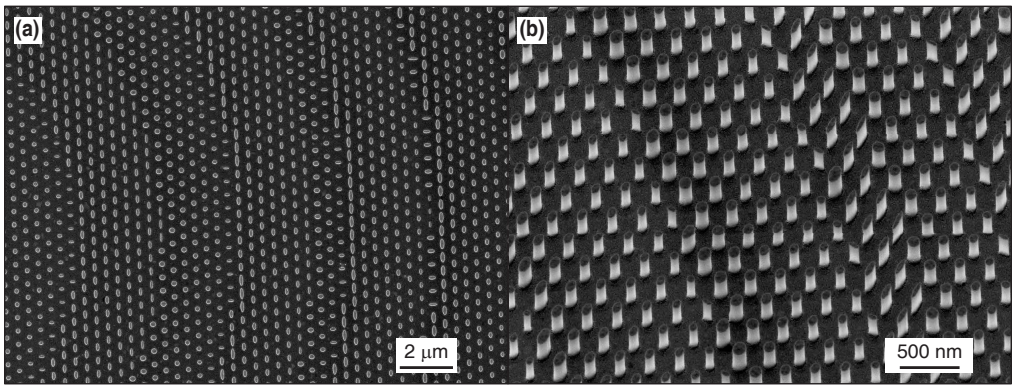

Fig. 3. (a) Scanning electron micrograph of a fabricated device viewed normally, and (b) at a tilt angle.

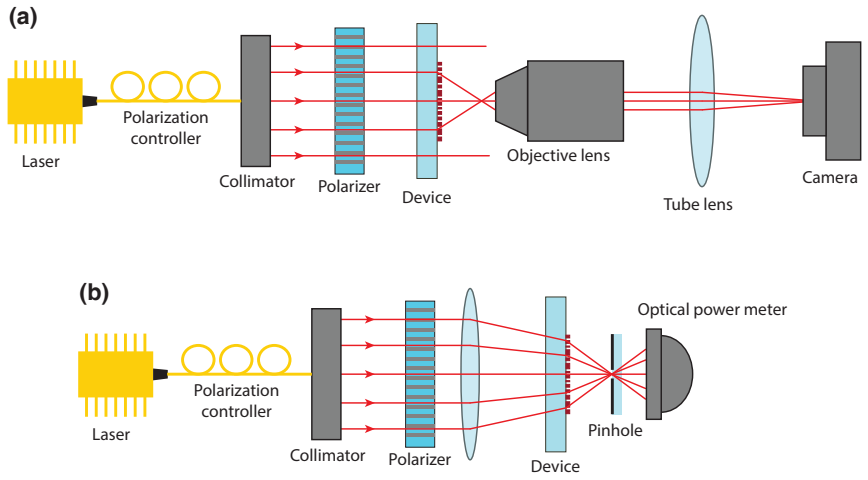

Fig. 4. (a) Schematic of the measurement setup used for measuring intensity profiles, and (b) focusing efficiencies.

measurements. Diameters of the used pinholes were 6, 6, 10, 15, and 20 μm for different lenses in decreasing NA order. We attribute the lower efficiency at 780 nm to higher sensitivity of its phase to fabrication errors.

We have also characterized the operation of the devices under illumination with cross-polarized light (i.e. y-polarized light at 915 nm, and x-polarized light at 780 nm). In cross-polarized operation, the devices also exhibit Fresnel phase zones but these zones are not optimized for focusing to a tight spot. Indeed, the cross-polarization measurement results summarized in Fig. 6 show that the devices focus cross-polarized light as well, but with lower efficiency, higher distortions, and to focal distances different from the corresponding copolarized values. It is worth noting that these devices operate as diffractive lenses with different phase profiles for x and y-polarized light. Also, for each polarization they follow the regular chromatic dispersion of diffractive lenses, and therefore their focal distance changes with wavelength proportional to $1/\lambda$ [23, 24, 26]. Since cross-polarized light is focused to a different focal distance, it can be considered as loss when the device focuses unpolarized light. When the devices are used for imaging applications, the excitation and the collected paths need to be passed through polarizers. Otherwise, the image will exhibit elevated background and/or imaging artifacts depending on the exact lens design.

Optics EXPRESS

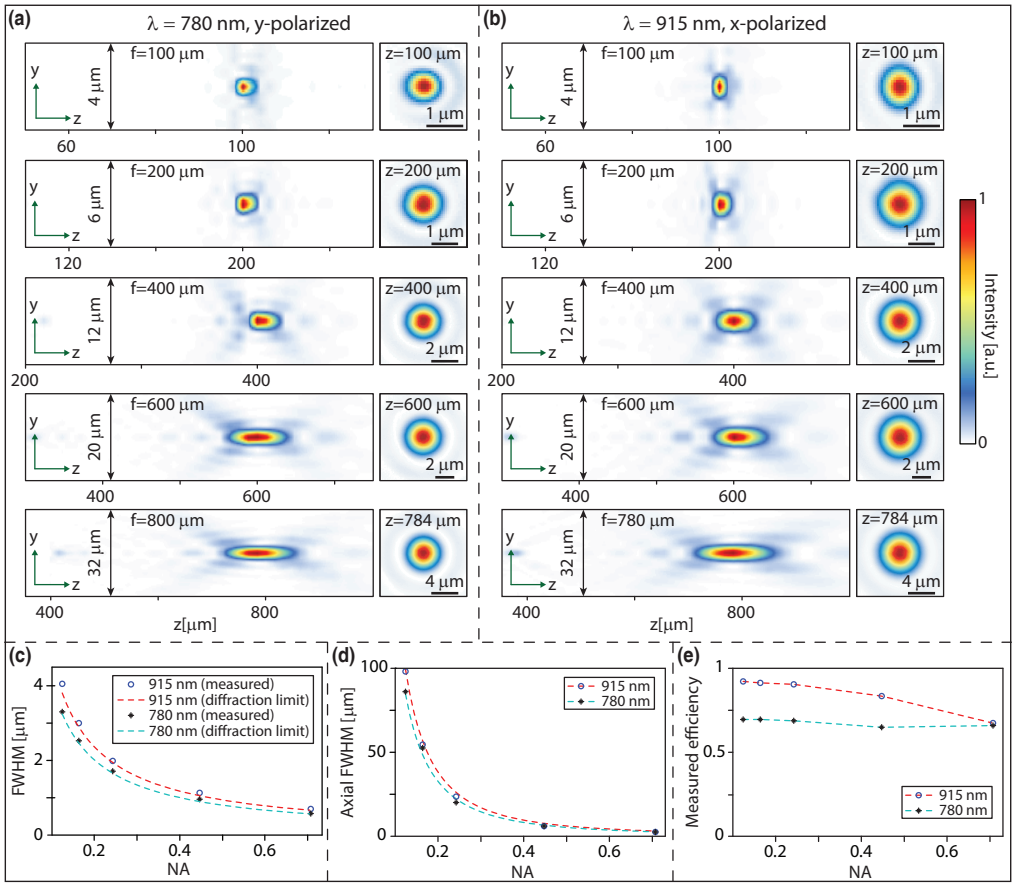

Fig. 5. (a) Measured axial (left) and focal (right) plane intensities for *y*-polarized light at 780 nm. Results are in increasing focal distance order from top to bottom. (b) Same measurement results as in (a) for *x*-polarized light at 915 nm. (c) Measured full width at half maximums in the focal plane versus NA. The corresponding theoretical diffraction limits at both wavelengths are denoted via dashed lines. (d) Measured axial plane FWHMs along with their corresponding theoretical values. (e) Measured efficiencies of the metasurface lenses at both wavelengths. Dashed lines show eye-guides.

Optics EXPRESS

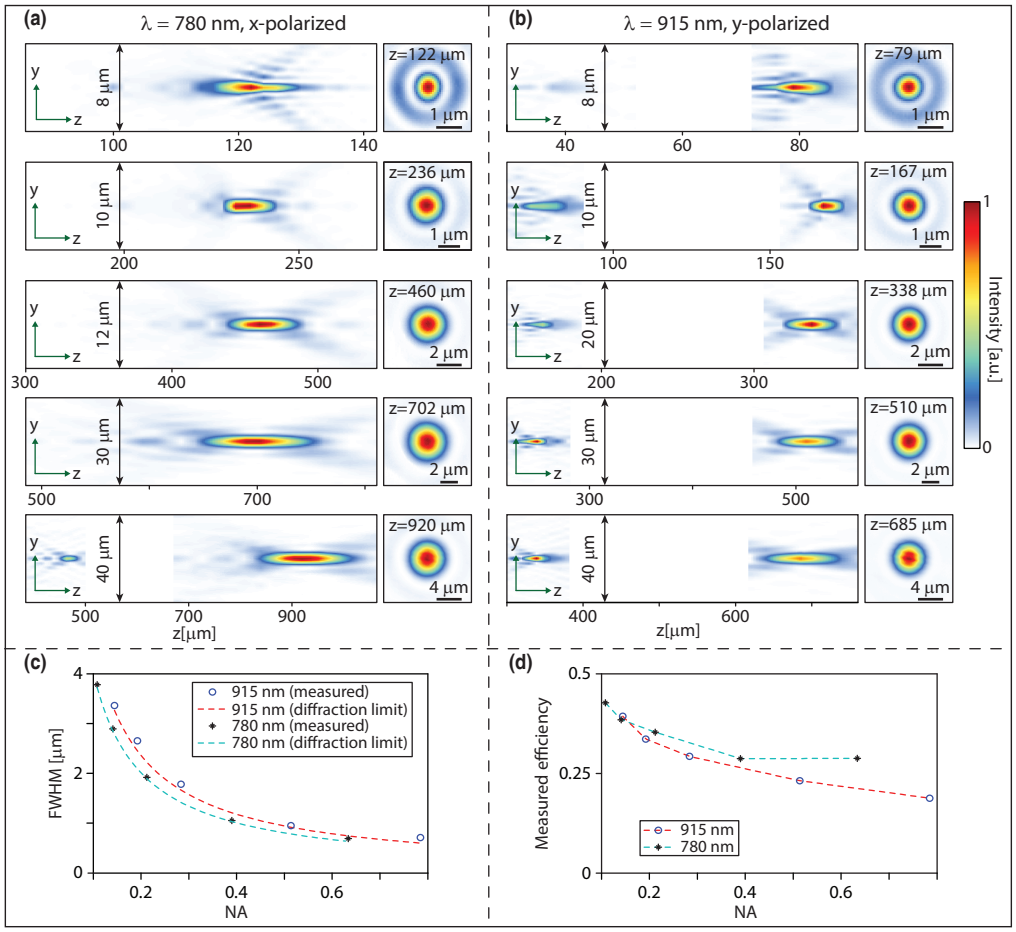

Fig. 6. Measurement results under illumination with cross-polarized light. (a) Measured axial (left) and focal (right) plane intensities for *x*-polarized light at 780 nm. Results are in increasing copolarized focal distance order from top to bottom. We have verified that no other points of comparable intensity are present in areas not shown in the axial measurements. (b) Same measurement results as in (a) for *y*-polarized light at 915 nm. (c) Measured full width at half maximums in the focal plane (focal distances labeled in (a) and (b)) versus NA. The corresponding theoretical diffraction limits at both wavelengths are denoted via dashed lines. (d) Measured efficiencies of the metasurface lenses at both wavelengths for cross-polarized light. Dashed lines show eye-guides.

The high NA and high efficiency, in addition to the fact that the working wavelengths can be arbitrarily close, make this platform attractive for single photon fluorescence microscopy where the two working wavelengths (i.e. the excitation and emission wavelengths of the fluorophores) are usually close [33]. In addition, these lenses can be used for light collection in cases where the sample is tagged with two different fluorophores with close emission spectra. It should be noted, however, that the efficiencies of the lenses will be 50% lower for unpolarized light, as the cross-polarized light will be focused to a different focal distance than the copolarized light [Figs. 5 and 6]. Besides, the lenses discussed here are aspherical and suffer from aberrations for off-axis imaging and focusing. This problem can be solved by designing lens doublets that are corrected for the off-axis monochromatic aberrations [34].

Optics EXPRESS

The maximum distance between the two operating wavelengths of the proposed metasurface platform is limited by practical considerations. The nano-posts height should be large enough to provide the required 2π phase at the longer wavelength. This results in higher sensitivity of the phases of nano-posts at the shorter wavelength to fabrication errors, which in turn decreases device efficiency at that wavelength. This lower efficiency at the shorter wavelength is already observed in this work. Thus, the maximum wavelength distance is limited mostly by practical considerations and the achievable fabrication tolerances.

In conclusion, birefringent elliptical nano-posts can be used to independently control optical wavefronts at two different wavelengths with orthogonal linear polarizations. This control can be utilized to generate any desired wavefronts at both wavelengths, resulting in an optical behavior at each wavelength independent from the other one. Using these meta-atoms, we demonstrated double-wavelength metasurface lenses that focus *x* and *y*-polarized light at 915 and 780 nm, respectively, to the same focal distance. Lenses with NA values up to 0.7 were experimentally demonstrated to have nearly diffraction limited operation and efficiencies above 65%. This method can also be combined with the recently demonstrated meta-molecule concept [26] to achieve more phase control parameters, and chromatically corrected lenses at four or more wavelengths.

Funding

This work was supported by Samsung Electronics. A.A. was also supported by National Science Foundation (NSF) award 1512266. S.M.K. was supported by the U.S. Department of Energy (DOE) “Light-Material Interactions in Energy Conversion” Energy Frontier Research Center under grant DE-SC0001293.

Acknowledgments

The devices were fabricated at the Kavli Nanoscience Institute at Caltech.